Opto-Electronic Advances

Article

February 2024, Vol. 7, No. 2

DOI: 10.29026/oea.2024.230171

Miniature tunable Airy beam optical meta-device

Jing Cheng Zhang[1†], Mu Ku Chen[1,2,3†], Yubin Fan[1†], Qinmiao Chen[4†], Shufan Chen[1], Jin Yao[1], Xiaoyuan Liu[1], Shumin Xiao[4*] and Din Ping Tsai[1,2,3*]

Tunable Airy beams with controllable propagation trajectories have sparked interest in various fields, such as optical manipulation and laser fabrication. Existing research approaches encounter challenges related to insufficient compactness and integration feasibility, or they require enhanced tunability to enable real-time dynamic manipulation of the propagation trajectory. In this work, we present a novel method that utilizes a dual metasurface system to surpass these limitations, significantly enhancing the practical potential of the Airy beam. Our approach involves encoding a cubic phase profile and two off-axis Fresnel lens phase profiles across the two metasurfaces. The validity of the proposed strategy has been confirmed through simulation and experimental results. The proposed meta-device addresses the existing limitations and lays the foundation for broadening the applicability of Airy beams across diverse domains, encompassing light-sheet microscopy, laser fabrication, optical tweezers, etc.

Keywords: metasurface; miniature device; tunable Airy beam; tunable meta-device

Zhang JC, Chen MK, Fan YB et al. Miniature tunable Airy beam optical meta-device. *Opto-Electron Adv* **7**, 230171 (2024).

Introduction

Airy beams have inspired tremendous research for their exotic properties, such as diffraction-free, self-accelerating, and self-healing[1]. The demand for generating tunable Airy beams has steadily increased since their discovery, driven by the controlled trajectories[2–4]. It sparked growing research interest across diverse applications[5], including optical manipulation[6,7] and laser fabrication[8]. In the traditional configuration, an optical tweezer is propelled by a tightly focused Gaussian beam to produce an optical gradient force, which serves to confine particles within a limited range of just a few micrometers, primarily because of the relatively short Rayleigh lengths[7]. In contrast, the precisely controlled propagation trajectory of the Airy beam enables the optical manipulation of particles in air or liquid along designated paths and provides the capability to navigate obstacles. These beams can also facilitate the creation of surfaces with desired curvatures and enhance the adaptability of laser fabrication. While the feasibility of demonstrating these

[1]Department of Electrical Engineering, City University of Hong Kong, Kowloon, Hong Kong SAR 999077, China; [2]State Key Laboratory of Terahertz and Millimeter Waves, City University of Hong Kong, Kowloon, Hong Kong SAR 999077, China; [3]Centre for Biosystems, Neuroscience, and Nanotechnology, City University of Hong Kong, Kowloon, Hong Kong SAR 999077, China; [4]Ministry of Industry and Information Technology Key Lab of Micro-Nano Optoelectronic Information System, Guangdong Provincial Key Laboratory of Semiconductor Optoelectronic Materials and Intelligent Photonic Systems, Harbin Institute of Technology, Shenzhen 518055, China.

[†]These authors contributed equally to this work.

*Correspondence: SM Xiao, E-mail: shumin.xiao@hit.edu.cn; DP Tsai, E-mail: dptsai@cityu.edu.hk

Received: 21 September 2023; Accepted: 15 November 2023; Published online: 2 February 2024

applications has been established, the Airy beam still requires certain tunable characteristics to enhance its practical utility.

Airy beams were traditionally generated by bulky and costly optical devices, such as complex optical lens system[9], spatial light modulators (SLM)[10], etc. These methods offer the capability to achieve tunable Airy beams. Utilizing a complex optical lens system generates tunable Airy beams by manipulating the tilt angle of cylindrical telescopic systems. SLMs are diffractive devices engineered to create tunable Airy beams by performing pixel-level phase changes. While these methods offer a degree of Airy beam control, each method comes with its challenges. The intricate optical setup inevitably encounters difficulties in achieving precise alignment. SLMs face challenges such as low conversion efficiency, restricted resolution, and limitations related to incident polarization and power. These techniques also struggle to enable the realization of compact and integrated optical systems due to the utilization of bulky components.

Metasurface is an advanced flat optical device composed of artificial nano-antennas[11–16]. It offers an unusual way to engineer the light's amplitude[17,18], phase[19,20], wavelength[21–23], polarization[24–26], orbital angular momentum[27], etc. Numerous functions and applications have been developed based on ultrathin optical devices[28–35], such as meta-lenses[36–39], nonlinear meta-lens[40], orbital angular momentum manipulation[41–43], logic gate[44], polarization control and measurement[25], structural color[45], single-shot phase-imaging devices[46–48] and other novel meta-devices[49]. It is thus an ultra-compact and flat technique for Airy beam generation[4,50–55]. For example, Lei et al. demonstrated a series of Airy beams with different trajectories by combining the cubic phase with different lens profiles[4]; Lu et al. showed a way to control the trajectories of the Airy beams by integrating the cubic phase and a gradient phase into a single metasurface[50]. While the currently demonstrated works offer a variety of methodologies for manipulating the propagation trajectory or the focal spot position of the Airy beam in a compact way, real-time tuning of the generated Airy beam remains challenging.

In this work, we demonstrate a novel method for generating tunable Airy beams using a bilayer all-dielectric meta-device. It is meticulously crafted by integrating and rotating various phase profiles, including the cubic phase and two off-axis Fresnel lens phase profiles. By leveraging the transmission phase properties of the nanoantennas at specific positions, the meta-device effectively functions as a tunable optical wavefront modulator, showing the capacity of tunable trajectory manipulation. This inventive approach allows us to dynamically manipulate the trajectories of Airy beams by rotating these two metasurfaces, as shown in Fig. 1. We conduct experimental investigations on a proof-of-concept meta-device to validate its viability and flexibility. Our experimental findings align well with the theoretically predicted intensity profiles and propagation dynamics of the Airy beam.

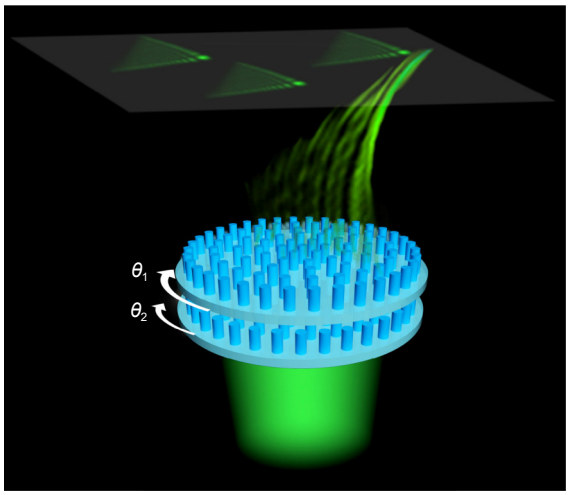

Fig. 1 | Schematic of all-dielectric meta-device for generating dynamic Airy beam.

Results and discussion

We implement the all-dielectric meta-device as follows: a combination of a cubic phase and one of the Fresnel holographic lens phases is applied to one metasurface, while the other metasurface is equipped with another Fresnel holographic lens phase. Note that the two Fresnel holographic lens phases are both off-axis and have opposite focal lengths. The generation of Airy beams involves performing a Fourier transformation on Gaussian beams that propagate through the metasurface exhibiting cubic phase modulation. A tunable gradient phase can be achieved by superimposing these two off-axis Fresnel holographic lenses. The tunable gradient phase enables the flexible modulation of the Airy beam in response to varying propagation trajectories in the longitudinal direction and focal spot locations in the transverse plane. We opted to utilize Fresnel holographic lenses instead of directly employing two gradient phases[19] due to the benefits of focusing phases. Focusing phases can mitigate losses caused by the divergence of

the light beam during propagation, ensuring optimal transmission through the first metasurface and facilitating its subsequent passage to the second metasurface.

The Airy beams are generated by the Fourier transformation of Gaussian beams combined with cubic phase, and the transverse field distribution, $h(u,v)$, can be written as[4]

$$h(u,v,z=0) = Ai\left(\frac{u}{u_0}\right)\exp\left(a\frac{u}{u_0}\right) \cdot Ai\left(\frac{v}{v_0}\right)\exp\left(a\frac{v}{v_0}\right), \quad (1)$$

where $Ai(u, v)$ is the Airy function, a is a constant. (u, v) are dimensionless transverse coordinates of the Airy beam. (u_0, v_0) is an arbitrary transverse scale. By careful calculation, the Fourier transform of the above Airy beam at the origin, $H(x, y)$, could be written as

$$H(x,y) = b^2\exp\left[\frac{\mathrm{i}(2\pi b)^3(x^3+y^3)}{3}\right], \quad (2)$$

where b is a constant with units of m^{-1}; i is the imaginary unit; (x,y) is spatial frequencies in the Fourier frequency domain. Now we get the cubic phase $\phi(x_{\mathrm{meta}}, y_{\mathrm{meta}})$ for Airy beam generation with metasurface, which is

$$\phi = \frac{(2\pi b)^3\left({x_{\mathrm{meta}}}^3+{y_{\mathrm{meta}}}^3\right)}{3}, \quad (3)$$

where, $(x_{\mathrm{meta}}, y_{\mathrm{meta}})$ is the coordinate of the metasurface phase plane.

The tunable gradient phase could be obtained using two Fresnel holographic lens phases, which are both off-axis and have opposite focal lengths. One phase profile has a positive focal length of f_d and a displacement of d to $+x$ direction. The other has a corresponding negative focal length and a displacement to the left. We also assume that the first Fresnel holographic lens phase is rotated counter-clockwise by an angle of $\theta/2$ around the central axis, the other symmetrically clockwise by an angle $-\theta/2$. Then, the corresponding phase profiles P_1 and P_2 can be written as[56]

$$P_1 = -\frac{\pi}{\lambda_d f_d}\left(\left[x_{\mathrm{meta}}+d\cos\frac{\theta}{2}\right]^2+\left[y_{\mathrm{meta}}-d\sin\frac{\theta}{2}\right]^2\right), \quad (4)$$

$$P_2 = \frac{\pi}{\lambda_d f_d}\left(\left[x_{\mathrm{meta}}-d\cos\frac{\theta}{2}\right]^2+\left[y_{\mathrm{meta}}+d\sin\frac{\theta}{2}\right]^2\right), \quad (5)$$

where λ_d is the design wavelength of the two Fresnel holographic lenses. Adding the two phases, we could get the total phase profile P_{tot}, which is

$$P_{\mathrm{tot}} = -4d\frac{\pi}{\lambda_d f_d}\cos\frac{\theta}{2}x_{\mathrm{meta}}, \quad (6)$$

We get a phase gradient with a grating vector $\boldsymbol{G}$,

$$\boldsymbol{G} = 4d\frac{\pi}{\lambda_d f_d}\cos\frac{\theta}{2}\boldsymbol{e_x}, \quad (7)$$

where $\boldsymbol{e_x}$ is a unit vector in the x-direction. Then, the beam deflection angle β in x-direction of a normal incident light will be,

$$\beta = \arcsin\left[\frac{|\boldsymbol{G}|\,\lambda}{2\pi}\right] = \arcsin\left[\frac{2d\lambda}{\lambda_d f_d}\cos\frac{\theta}{2}\right]. \quad (8)$$

Here, λ is the working wavelength. We can find that the magnitude of the phase gradient depends on the metasurface's rotation angles, and parameters of the off-axis Fresnel holographic lens phases determine the maximum magnitude. The theoretically achievable zone is constrained once the meta-device has been manufactured. These achievable zones can be tailored to suit specific applications by tuning the parameters of the phase profiles before fabrication. We account for more realistic conditions in the simulation and experiment section. Initially, we compute the complex amplitude (E_1) when light is about to impinge on the second metasurface (1 mm away from the first one), and subsequently determine the complex amplitude (E_2) after passing through the second metasurface. We then employ E_2 as the new source for calculating the Airy beam distribution. Without any mathematical approximation, the experiment setup is consistent with the simulation to obtain excellent agreement.

For a compact meta-device design, we set the phase profile P_1 for the first metasurface (near the incident light) and combine the cubic phase profile ϕ and the off-axis Fresnel holographic lens profile P_2 to form the phase of the second metasurface. When the phases of two metasurfaces superimpose, the squared terms of the respective focused phases nullify each other, leading to a gradient phase related to the rotational angle. As a result, the outcome comprises a cubic phase profile and a tunable gradient phase, as shown in Fig. S1. We set b to 2.5 and $\pi/(f_d\lambda_d)$ to 220 and subsequently fabricated the sample as a proof-of-concept meta-device. With the tunable grating, the Airy beam can be tuned dynamically as designed, i.e., the propagation trajectories and focal spots of the Airy beams can be controlled flexibly.

The meta-device comprises arrays of amorphous

titanium dioxide (TiO_2) cylindrical nanorods of different diameters and fixed height (800 nm) on a glass substrate. The period (p) is 300 nm and the diameters of the metasurfaces are both 1 mm. We choose TiO_2 due to its high refractive index, minimal surface roughness, and high transmission at visible frequency[57–59]. Figure 2(a) shows the optical characteristics of the designed nanoantenna of the meta-device obtained through COMSOL Multiphysics®. The working wavelength is 532 nm, the phase can cover 2π when the diameter varies gradually from 50 nm to 113 nm, and the efficiency of the selected nanoantennas is higher than 90%. Insert shows the schematic of the nanoantenna. Figure 2(b–d) shows the designed phase profile, optical image, and the measured phase profile of the first metasurface, respectively. Figure 2(e–g) shows the designed phase profile, optical image, and the measured phase profile of the second metasurface, respectively. The phase profile is measured using MetronLens from Ideaoptics Co., Ltd, Shanghai. Figure 2(h–i) shows scanning electron microscope (SEM) images of the meta-device. The fabrication process is shown in Fig. S2. Our results substantiate a high degree of congruence between design and fabrication.

We first provide two sets of detailed comparisons between simulation and experimental results to validate our design and fabrication, as shown in Fig. 2(a–c) and Fig. 2(d–f), respectively. The simulation method is based on the Fresnel diffraction algorithm[19]. The experimental setup can be found in Fig. S3. We will methodically present the comparative analysis of simulation and experimental results from three perspectives: the intensity distribution along the propagation of the Airy beam, the intensity distribution in the focal plane, and the intensity distribution along a single line passing through the

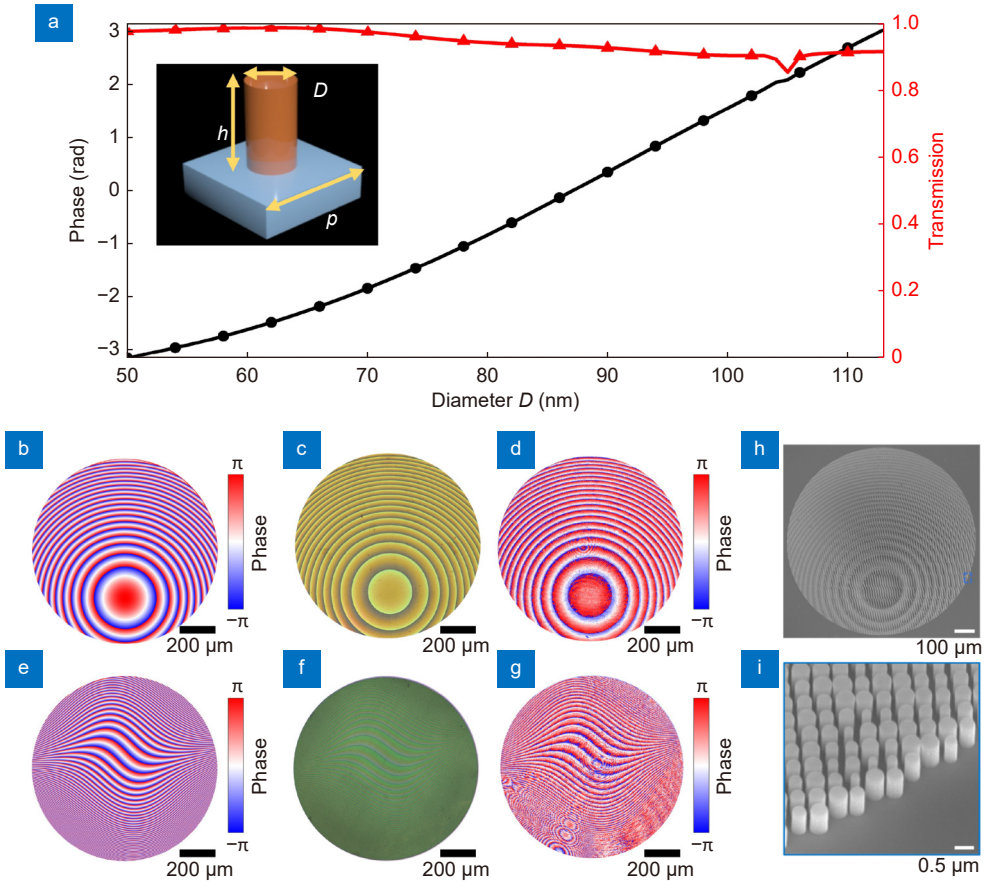

Fig. 2 | Characteristic of the meta-device. (**a**) The optical characteristics of the nanoantenna. The phase can encompass a complete 2π cycle as the diameter transitions from 50 nm to 113 nm, achieving an efficiency exceeding 90% for all the selected nanoantennas. The inset depicts the schematic of the nanoantenna. (**b**, **e**) The phase profiles of the first (b) and the second (e) metasurface. (**c**, **f**) The optical images of the fabricated metasurfaces according to the phase profile in (b) and (e), respectively. (**d**, **g**) The measured phase profiles of the fabricated metasurfaces. Scalar bars: 200 μm. The phase profile is measured using MetronLens from Ideaoptics Co., Ltd, Shanghai. (**h**) Scanning electron microscope (SEM) images of the meta-device. Scale bar: 100 μm. (**i**) Tiled-view (blue square) zoomed-in SEM image of meta-atoms of the metasurface. Scale bar: 0.5 μm.

focal spot. The rotation angles of the two metasurfaces are both zero in the case shown in Fig. 2(a). Figure 2(b) and 2(c) show the simulated and experimental intensity of the longitudinal distribution (left column), focal plane (upper right), and a line in the focal plane (lower right). The simulation and measured results match well with each other in all these aspects. Figure 2(d–f) illustrates the cases where the rotation angles for the two metasurfaces are -π/2 and π/2, respectively. The presented results further validate the accuracy of our design. The measured efficiency in the generation of Airy beams is approximately 15%. Upon practical implementation of the proposed meta-device, the separation between these two metasurfaces can be further minimized to mitigate diffraction losses during transmission. In both cases, the Airy beams were measured and exhibited a strong and clear agreement with the predicted results, showcasing distinct focal spots and controlled trajectories.

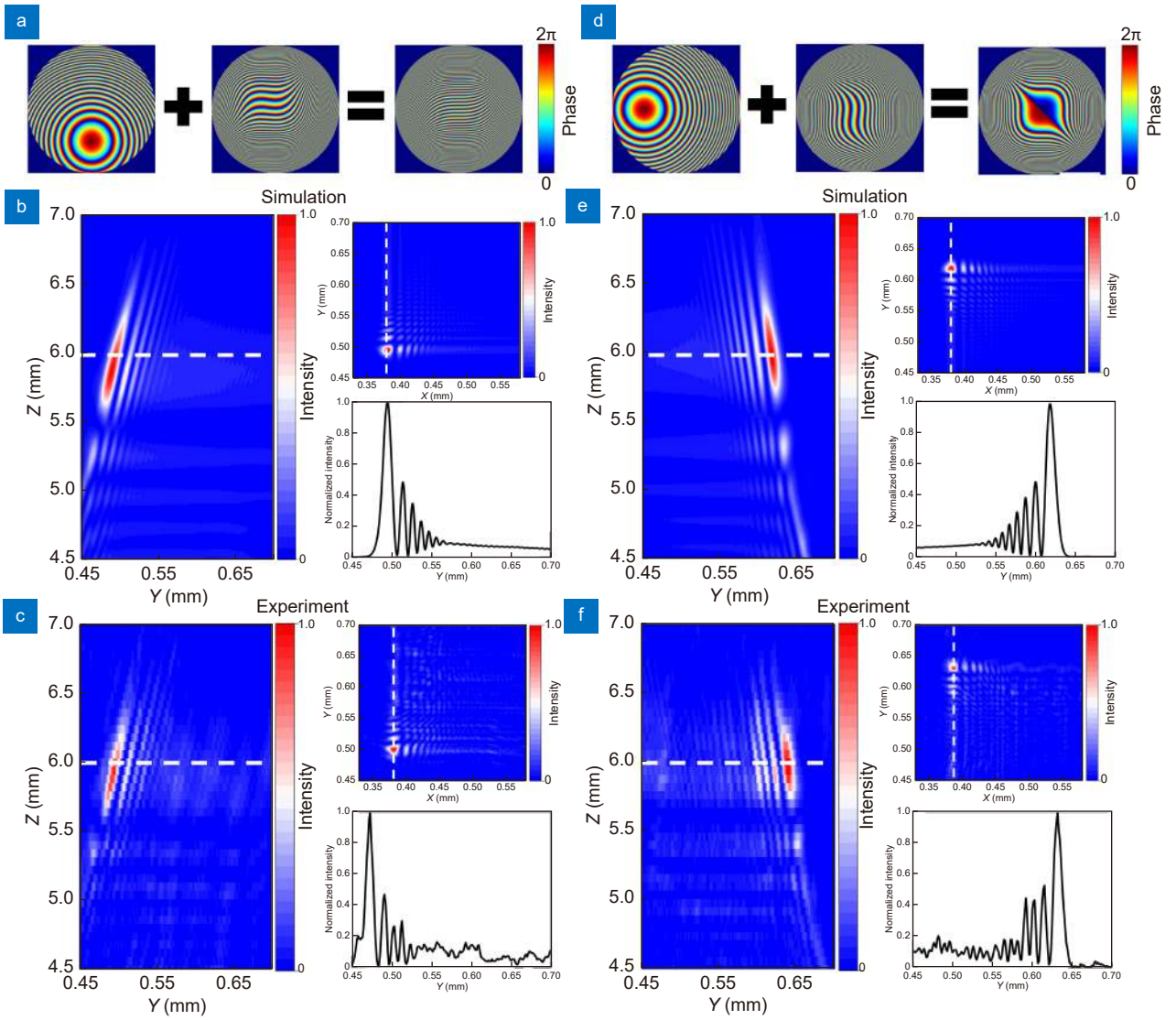

Fig. 3 | The simulated and experimental results of the meta-devices. (**a**) The phase obtained upon the superposition of the two metasurfaces when the rotation angles of the two metasurfaces are both zero. (**b**) The simulated results when the rotation angle is set as shown in (a). The left column shows the Airy beam intensity in the propagation direction, and the dashed line shows the focal plane. The intensity distribution of the focal plane is shown in the upper right. The lower right shows the intensity distribution of the line that crosses the focal spot indicated by the dashed line in the upper right. (**c**) The experimental results according to those shown in (b). (**d**) The phase obtained upon superposition of the two metasurfaces when the rotation angles are -π/2 and π/2, respectively. (**e**) The simulated results when the rotation angle is set as shown in (d). The left column shows the Airy beam intensity in the propagation direction, and the dashed line shows the focal plane. The intensity distribution of the focal plane is shown in the upper right. The Lower right shows the intensity distribution of the line that crosses the focal spot indicated by the dashed line in the upper right. (**f**) The experimental results according to those shown in (b).

Based on the simulation and experimental results depicted in Fig. 3, it is evident that the Airy beam exhibits the remarkable ability to sustain its focused state over a propagation distance of up to 0.5 mm, which is nearly 1000 times the working wavelength. This underscores the non-diffraction attribute of the Airy beam. In contrast to the conventional Gaussian beam, which, focusing, yields only a single focused spot that rapidly diverges, the non-diffraction property of the Airy beam guarantees the maintenance of focus and preservation of its initial shape and intensity distribution during propagation. This characteristic holds promise for applications in optical manipulation, such as nanoparticle transportation along its transmission path. The self-accelerating feature of Airy beams denotes the phenomenon wherein an Airy beam inherently bends and accelerates while traversing a curved trajectory, setting it apart from traditional Gaussian beams. This self-accelerating attribute is of great practical value in specific scenarios, especially in situations requiring obstacle avoidance or the tracing of complex light pathways. We posit that it can be applied effectively in laser manufacturing processes for nanostructures with curved surface profiles.

We present comprehensive experimental results in Fig. 4. The focal spots of the Airy beams achieved by rotating the metasurfaces are illustrated in Fig. 4(a). The relationship between the rotation angles and focal spot positions is listed in Table S1. From Fig. 4(a), we observe the flexibility of steering focal spots within the focal plane, implying diverse propagation trajectories. We have chosen several cases labeled with colored squares to demonstrate the intensity distribution across the focal planes, as depicted in Fig. 4(b), and the scalar bar is 20 μm. Airy beams with side lobes of different orientations are observed, increasing the manipulation flexibility of the propagation trajectories. This is reasonable because the rotation of the second metasurface determines the orientations of the side lobes of the Airy beams.

Conclusions

In summary, we have demonstrated a new method for tuning the Airy beam's focal spots and propagation trajectories for optical manipulation and laser manufacturing. The Airy beams can be tuned dynamically by rotating the meta-device once encoding a cubic phase profile and two off-axis Fresnel lens phase profiles into two cascading metasurfaces. The manipulation capacity of an Airy beam's propagation trajectory and coverage range can be easily achieved in demand by tuning the parameters of these phase profiles. Without enlarging the device footprint, our approach effectively enhances the modulation flexibility of Airy beams. Real-time rotation of metasurfaces can be performed by piezoelectricity, further strengthening the tunability and flexibility of our meta-devices. Compared with the traditional tilted cylindrical telescopic system or the SLM, the demonstrated meta-device significantly reduces the volumetric thickness and operational complexity and can be easily transferred to other working bands without polarization or other limitations. The proposed meta-device, taking advantage of miniaturization and easy control, can be compatible with other optical devices and holds promise for various applications.

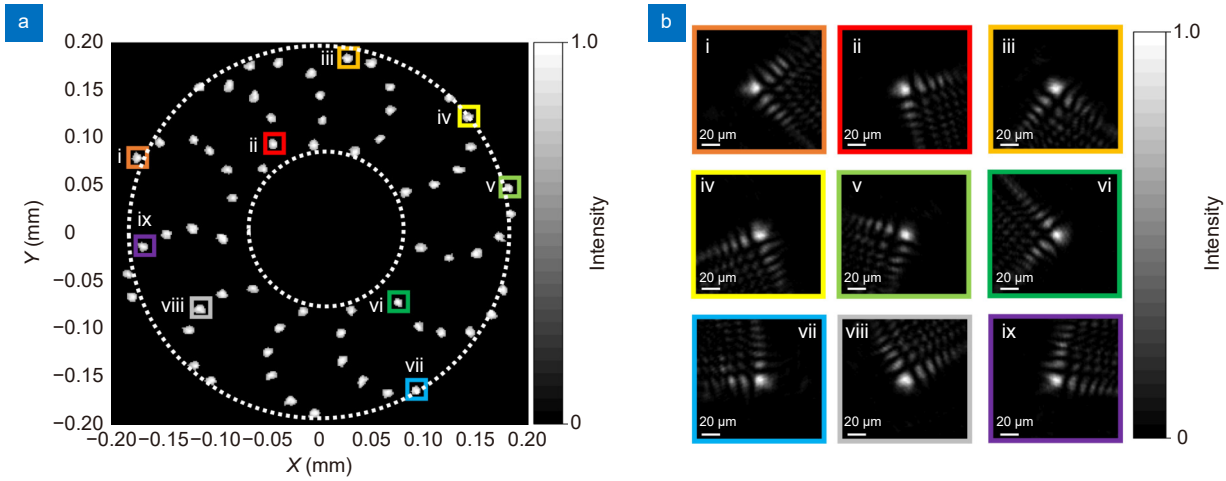

Fig. 4 | The experimental results of the meta-devices. (**a**) Different focal spots of the Airy beam when varying the rotation angles of the metasurfaces. The theoretically achievable zone is marked between the two dotted circles. (**b**) The intensity distributions of the focal plane selected from Fig. 4(a) are indicated by squares of different colors. Scalar bar: 20 μm.

References

1. Siviloglou GA, Broky J, Dogariu A et al. Observation of accelerating airy beams. *Phys Rev Lett* **99**, 213901 (2007).
2. Ellenbogen T, Voloch-Bloch N, Ganany-Padowicz A et al. Nonlinear generation and manipulation of airy beams. *Nat Photonics* **3**, 395–398 (2009).
3. Li Z, Liu WW, Geng GZ et al. Multiplexed nondiffracting nonlinear metasurfaces. *Adv Funct Mater* **30**, 1910744 (2020).
4. Wen J, Chen L, Yu BB et al. All-dielectric synthetic-phase metasurfaces generating practical airy beams. *ACS Nano* **15**, 1030–1038 (2021).
5. Efremidis NK, Chen ZG, Segev M et al. Airy beams and accelerating waves: an overview of recent advances. *Optica* **6**, 686–701 (2019).
6. Gao DL, Ding WQ, Nieto-Vesperinas M et al. Optical manipulation from the microscale to the nanoscale: fundamentals, advances and prospects. *Light Sci Appl* **6**, e17039 (2017).
7. Kuo HY, Vyas S, Chu CH et al. Cubic-phase metasurface for three-dimensional optical manipulation. *Nanomaterials* **11**, 1730 (2021).
8. Manousidaki M, Papazoglou DG, Farsari M et al. Abruptly autofocusing beams enable advanced multiscale photo-polymerization. *Optica* **3**, 525–530 (2016).
9. Papazoglou DG, Suntsov S, Abdollahpour D et al. Tunable intense airy beams and tailored femtosecond laser filaments. *Phys Rev A* **81**, 061807 (2010).
10. Wang J, Hua XW, Guo CL et al. Airy-beam tomographic microscopy. *Optica* **7**, 790–793 (2020).
11. Chen MK, Liu XY, Sun YN et al. Artificial intelligence in metaoptics. *Chem Rev* **122**, 15356–15413 (2022).
12. Yao J, Lin R, Chen MK et al. Integrated-resonant metadevices: a review. *Adv Photonics* **5**, 024001 (2023).
13. Chen MK, Wu YF, Feng L et al. Principles, functions, and applications of optical meta‐lens. *Adv Opt Mater* **9**, 2001414 (2021).
14. Li T, Chen C, Xiao XJ et al. Revolutionary meta-imaging: From superlens to metalens. *Photonics Insights* **2**, R01 (2023).
15. Ma Q, Liu C, Xiao Q et al. Information metasurfaces and intelligent metasurfaces. *Photonics Insights* **1**, R01 (2022).
16. Xu Q, Lang YH, Jiang XH et al. Meta-optics inspired surface plasmon devices. *Photonics Insights* **2**, R02 (2023).
17. Wang Z, Liang Y, Qu JQ et al. Plasmonic bound states in the continuum for unpolarized weak spatially coherent light. *Photonics Res* **11**, 260–269 (2023).
18. Liang Y, Koshelev K, Zhang FC et al. Bound states in the continuum in anisotropic plasmonic metasurfaces. *Nano Lett* **20**, 6351–6356 (2020).
19. Zhang JC, Wu GB, Chen MK et al. A 6g meta-device for 3d varifocal. *Sci Adv* **9**, eadf8478 (2023).
20. Georgi P, Wei QS, Sain B et al. Optical secret sharing with cascaded metasurface holography. *Sci Adv* **7**, eabf9718 (2021).
21. Li X, Chen QM, Zhang X et al. Time-sequential color code division multiplexing holographic display with metasurface. *Opto-Electron Adv* **6**, 220060 (2023).
22. Liu J, Shi MM, Chen Z et al. Quantum photonics based on metasurfaces. *Opto-Electron Adv* **4**, 200092 (2021).
23. Semmlinger M, Tseng ML, Yang J et al. Vacuum ultraviolet light-generating metasurface. *Nano Lett* **18**, 5738–5743 (2018).
24. Ma XL, Pu MB, Li X et al. All-metallic wide-angle metasurfaces for multifunctional polarization manipulation. *Opto-Electron Adv* **2**, 180023 (2019).
25. Wu PC, Tsai WY, Chen WT et al. Versatile polarization generation with an aluminum plasmonic metasurface. *Nano Lett* **17**, 445–452 (2017).
26. Chen WT, Török P, Foreman MR et al. Integrated plasmonic metasurfaces for spectropolarimetry. *Nanotechnology* **27**, 224002 (2016).
27. Wu GB, Chan KF, Shum KM et al. Millimeter-wave holographic flat lens antenna for orbital angular momentum multiplexing. *IEEE Trans Antennas Propag* **69**, 4289–4303 (2021).
28. Zhang JC, Chen MK, Liang Y et al. Nanoimprint meta‐device for chiral imaging. *Adv Funct Mater* **33** (2023).
29. Fan YB, Tonkaev P, Wang YH et al. Enhanced multiphoton processes in perovskite metasurfaces. *Nano Lett* **21**, 7191–7197 (2021).
30. Fan YB, Wang YH, Zhang N et al. Resonance-enhanced three-photon luminesce via lead halide perovskite metasurfaces for optical encoding. *Nat Commun* **10**, 2085 (2019).
31. Chen J, Wang DP, Si GY et al. Planar peristrophic multiplexing metasurfaces. *Opto-Electron Adv* **6**, 220141 (2023).
32. Chen ZK, Hong MH. All-optical vector visual cryptography with high security and rapid decryption. *Opto-Electron Adv* **6**, 230073 (2023).
33. Yao J, Ou JY, Savinov V et al. Plasmonic anapole metamaterial for refractive index sensing. *PhotoniX* **3**, 23 (2022).
34. Wu GB, Dai JY, Shum KM et al. A universal metasurface antenna to manipulate all fundamental characteristics of electromagnetic waves. *Nat Commun* **14**, 5155 (2023).
35. Wu GB, Dai JY, Cheng Q et al. Sideband-free space–time-coding metasurface antennas. *Nat Electron* **5**, 808–819 (2022).
36. Wang SM, Wu PC, Su VC et al. A broadband achromatic metalens in the visible. *Nat Nanotechnol* **13**, 227–232 (2018).
37. Luo Y, Tseng ML, Vyas S et al. Meta-lens light-sheet fluorescence microscopy for *in vivo* imaging. *Nanophotonics* **11**, 1949–1959 (2022).
38. Gao H, Fan XH, Wang YX et al. Multi-foci metalens for spectra and polarization ellipticity recognition and reconstruction. *Opto-Electron Sci* **2**, 220026 (2023).
39. Pu MB, Li X, Guo YH et al. Nanoapertures with ordered rotations: Symmetry transformation and wide-angle flat lensing. *Opt Express* **25**, 31471–31477 (2017).
40. Tseng ML, Semmlinger M, Zhang M et al. Vacuum ultraviolet nonlinear metalens. *Sci Adv* **8**, eabn5644 (2022).
41. Gao H, Fan XH, Wang YX et al. Metasurface‐based orbital angular momentum multi‐dimensional demultiplexer and decoder. *Laser Photonics Rev* **17**, 2300393 (2023).
42. Pu MB, Li X, Ma XL et al. Catenary optics for achromatic generation of perfect optical angular momentum. *Sci Adv* **1**, e1500396 (2015).
43. Guo YH, Zhang SC, Pu MB et al. Spin-decoupled metasurface for simultaneous detection of spin and orbital angular momenta via momentum transformation. *Light Sci Appl* **10**, 63 (2021).
44. Huang YJ, Xiao TX, Chen S et al. All-optical controlled-not logic gate achieving directional asymmetric transmission based on metasurface doublet. *Opto-Electron Adv* **6**, 220073 (2023).
45. Yang WH, Xiao SM, Song QH et al. All-dielectric metasurface for high-performance structural color. *Nat Commun* **11**, 1864 (2020).
46. Kwon H, Arbabi E, Kamali SM et al. Single-shot quantitative

phase gradient microscopy using a system of multifunctional metasurfaces. *Nat Photonics* **14**, 109–114 (2020).
47. Engay E, Huo D, Malureanu R et al. Polarization-dependent all-dielectric metasurface for single-shot quantitative phase imaging. *Nano Lett* **21**, 3820–3826 (2021).
48. Wu QY, Zhou JX, Chen XY et al. Single-shot quantitative amplitude and phase imaging based on a pair of all-dielectric metasurfaces. *Optica* **10**, 619–625 (2023).
49. Luo Y, Chu CH, Vyas S et al. Varifocal metalens for optical sectioning fluorescence microscopy. *Nano Lett* **21**, 5133–5142 (2021).
50. Wang HY, Du J, Wang H et al. Generation of spin - dependent accelerating beam with geometric metasurface. *Adv Opt Mater* **7**, 1900552 (2019).
51. Cheng QQ, Wang JC, Ma L et al. Achromatic terahertz airy beam generation with dielectric metasurfaces. *Nanophotonics* **10**, 1123–1131 (2021).
52. Yu BB, Wen J, Chen L et al. Polarization-independent highly efficient generation of airy optical beams with dielectric metasurfaces. *Photonics Res* **8**, 1148–1154 (2020).
53. Zhang S, Xue H, Zhao SH et al. Generation and modulation of a two-dimensional airy beam based on a holographic tensor metasurface. *Phys Rev Appl* **18**, 064085 (2022).
54. Miao ZW, Hao ZC, Jin BB et al. Low-profile 2-D THz airy beam generator using the phase-only reflective metasurface. *IEEE Trans Antennas Propag* **68**, 1503–1513 (2020).
55. Luo Y, Tseng ML, Vyas S et al. Metasurface-based abrupt autofocusing beam for biomedical applications. *Small Methods* **6**, 2101228 (2022).
56. Bawart M, Bregenzer N, Bernet S et al. Dynamic beam-steering by a pair of rotating diffractive elements. *Opt Commun* **460**, 125071 (2020).
57. Wu YK, Yang WH, Fan YB et al. TiO_2 metasurfaces: from visible planar photonics to photochemistry. *Sci Adv* **5**, eaax0939 (2019).
58. Sun S, Yang WH, Zhang C et al. Real-time tunable colors from microfluidic reconfigurable all-dielectric metasurfaces. *ACS Nano* **12**, 2151–2159 (2018).
59. Che YH, Wang XT, Song QH et al. Tunable optical metasurfaces enabled by multiple modulation mechanisms. *Nanophotonics* **9**, 4407–4431 (2020).

Author contributions

D. P. Tsai proposed the original idea and supervised the project. Y. B. Fan, Q. M. Chen and S. M. Xian fabricated the samples. J. C. Zhang and M. K. Chen performed the measurements. J. C. Zhang, M. K. Chen, S. F. Chen, J. Yao, and X. Y. Liu analysed the data. J. C. Zhang and D. P. Tsai discussed and prepared the manuscript; all authors reviewed and commented on it.

Competing interests

The authors declare no competing financial interests.

Supplementary information

Supplementary information for this paper is available at https://doi.org/10.29026/oea.2024.230171

Scan for Article PDF